

ORIGINAL RESEARCH PAPER

## Highly active Fe-doped ZIF-8 nanocatalyst in electrochemical degradation of pharmaceutical pollutant in neutral environment

Shima Amani<sup>1</sup>, Mohammad Rostamizadeh<sup>1,\*</sup>, Ali Ghadimi<sup>2</sup>

<sup>1</sup> Department of Chemical Engineering, Sahand University of Technology, Tabriz, Iran

<sup>2</sup> Faculty of Petrochemicals, Iran Polymer and Petrochemical Institute, Tehran, Iran

Received: 2021-02-24

Accepted: 2021-03-27

Published: 2021-05-01

### ABSTRACT

In this study, zeolitic imidazolate framework (ZIF-8) nanocatalyst was synthesized by the thermal solvent method and doped by Fe species through the wet impregnation technique. The nanocatalysts were applied for the degradation of Phenazopyridine Hydrochloride (PHP) through the heterogeneous Electro-Fenton (HEF) process. The nanocatalysts were characterized by XRD, BET-BJH, FT-IR, FE-SEM, TEM, and acidimetric-alkalimetric titration techniques. The results showed the high surface area ( $1335 \text{ m}^2\text{g}^{-1}$ ) and homogenous dispersion of Fe species. The influence of different operating conditions was investigated, including pH level, nanocatalyst concentration, applied current, and PHP concentration. The optimum conditions for the HEF system over the Fe-ZIF-8 nanocatalyst were pH=7,  $0.2 \text{ g L}^{-1}$  of the Fe-ZIF-8 nanocatalyst, 100 mA, and 10 ppm of PHP concentration, which resulted in 99% PHP removal. The developed nanocatalyst had high reusability for the PHP removal in the HEF process. The results confirm the high potential of ZIF-8 nanocatalyst for pharmaceutical wastewater treatment through the HEF process.

**Keywords:** Water treatment; Electro-Fenton; Nanocatalyst; Metal-Organic Framework; ZIF-8

### How to cite this article

Amani Sh., Rostamizadeh M., Ghadimi A. Highly active Fe-doped ZIF-8 nanocatalyst in electrochemical degradation of pharmaceutical pollutant in neutral environment. J. Water Environ. Nanotechnol., 2021; 6(2): 138-149.

DOI: 10.22090/jwent.2021.02.004

### INTRODUCTION

Pharmaceutical pollutants threaten the health of humans, animals, and plants. Toxicity, non-biodegradability, and drug resistance have led to the use term “pseudo stable pollutants” for these compounds [1, 2]. Pharmaceutical compounds could create potential hazards for aquatic and terrestrial organisms by entering the environment and natural resources as well as direct contact with humans. Therefore, the need to develop suitable, inexpensive, fast, and recyclable wastewater treatment technologies is essential. One of these drug combinations is Phenazopyridine Hydrochloride (PHP) as an important aromatic compound. PHP is an analgesic drug and treats symptoms such as pain and burning in the urine, feeling of reflux, or

urine rejection due to stimulation of the mucous membrane of the lower urinary tract [3]. Exerted PHP into aquatic resources has harmful effects on the liver and other organs. Also, signs of cancer in mice were observed due to the prolonged use of PHP-contaminated water sources [4].

Among studied methods for wastewater treatment, advanced oxidation processes (AOPs) such as electro-Fenton (EF) have attracted great interest [5, 6]. EF is more suitable for treating wastewater containing pharmaceutical compounds owing to the great potential to complete pollutant elimination [7, 8]. EF processes is an indirect electrochemical method [9] in which free hydroxyl radicals ( $\text{OH}^{\cdot}$ ) are produced *in-situ* by means of electrical power in a mildly acidic environment. The need for transporting no hazardous materials

\* Corresponding Author Email: [rostamizadeh.m@gmail.com](mailto:rostamizadeh.m@gmail.com)

such as  $\text{H}_2\text{O}_2$ , no expensive equipment, and compact set-up are considered as the advantages of the EF process [10]. However, strict pH control for inhibiting iron sludge formation, loss of Fenton's reagent, and inability to recover aqueous  $\text{Fe}^{2+}$  as a catalyst is considered economic drawbacks that prevent practical scale-up of the homogeneous EF process [11]. The drawbacks could be potentially addressed by the utilization of a heterogeneous catalyst, such as iron minerals like pyrite, magnetite, hematite, and iron incorporated porous materials including clays, zeolites, and MOFs [12]. Metal-Organic Frameworks (MOFs) have regular structures that result from the bonding of minerals and organics [13]. The unique properties of these compounds such as high free surface, high thermal and mechanical strength, low density, and high porosity [14] have been widely considered by researchers in order to remove organic pollutants like coloring agents and pharmaceutical contaminants [15, 16].

Imidazolate zeolite frameworks (ZIF) are hybrid porous compounds that consist of four-faced units. These compounds are a bunch of MOFs in which the metal ions are zinc or cobalt cations and the connectors of the metal ions are imidazolate. Imidazole is an aromatic heterocyclic compound and a diazole group that converts to imidazolate by losing a proton in the presence of a strong basic [17]. The heterogeneous ZIF catalyst shows better thermal and hydrothermal stability than other types of MOFs [18]. Thi et al. [19] reported that iron loading on the ZIF-8 increased the adsorption capacity compared with the pure ZIF-8. Fe-ZIF-8 also showed faster kinetics than ZIF-8, while the presence of  $\text{Fe}^{2+}$  played a vital role in the effective elimination of Rubidium. The results showed that the maximum adsorption capacity of the Fe-ZIF-8 for the removal of colored compounds was  $193.96 \text{ mg g}^{-1}$ , which was 1.4 times more than the ZIF-8. Pan et al. [20] applied ZIF-67 to eliminate phenol and achieved the maximum phenol removal capacity of  $378.8 \text{ mg g}^{-1}$ . Wu et.al [21] applied ZIF-8 to remove arsenate. The results showed that zeolite ZIF-8 was a porous adsorbent with an excellent performance in removing arsenate and had a maximum adsorption capacity of  $12.287 \text{ mg g}^{-1}$ . Several studies have reported PHP removal using AOPs. Khataee et al. [22] reported that plasma-modified clinoptilolite (PMC) performance was more than natural clinoptilolite (NC) in optimum operational conditions, including  $\text{pH}=5$ , PMC

concentration of  $2 \text{ g L}^{-1}$ , ultrasonic power of 300 W, and 10 ppm PHP in heterogeneous sono-Fenton-like processes. PMC showed 90.14 % removal efficiency of PHP in 20 min. Eskandarloo et al. [23] studied the photocatalytic process using  $\text{Ag/SiO}_2\text{-TiO}_2$  nanoparticles and reported that PHP removal of 97.14 %. Abbasi et al. [24] studied HKUST-1 MOF for adsorption of PHP. Eskandarloo et al. [25] concluded that Sm-doped ZnO had higher PHP removal (59%) than pure ZnO (51%) in PHP degradation.

To the best of our knowledge, the utilization of Fe-doped ZIF-8 as heterogeneous nanocatalyst in the EF process has not been reported yet. In this research, we report the synthesis, characterization, and catalytic performance of the Fe-ZIF-8 nanocatalyst in the HEF process for the PHP removal. The effect of operating parameters of the HEF process, including wastewater pH, applied current, and nanocatalyst concentration was investigated.

## EXPERIMENTAL

### Materials

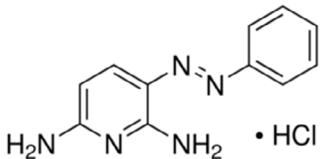
Zinc nitrate hexahydrate ( $\text{Zn}(\text{NO}_3)_2 \cdot 6\text{H}_2\text{O}$ ), 2-methylimidazole (Hmim,  $\text{C}_4\text{H}_6\text{N}_2$ ), ammonia ( $\text{NH}_3$ ), dimethylformamide (DMF,  $\text{C}_3\text{H}_7\text{NO}$ ), sulfuric acid ( $\text{H}_2\text{SO}_4$ ), sodium hydroxide (NaOH), iron chloride ( $\text{FeCl}_3 \cdot 6\text{H}_2\text{O}$ ), sodium sulfate ( $\text{Na}_2\text{SO}_4$ ), and sodium borohydride ( $\text{NaBH}_4$ ) were delivered by Merck Company (Germany). PHP as a model organic contaminant was kindly provided by the Shahre Daru pharmaceutical Company (Iran). Table 1 shows the general specification of PHP.

### Synthesis

The thermal solvent method was applied for the ZIF-8 synthesis. At the first step of the ZIF-8 synthesis procedure, 7.96 g of zinc nitrate hexahydrate was dissolved in 74.9 mL of ammonia. Then, 4.4 g of Hmim was dissolved in 80 mL of DMF. The resulted solutions were mixed and then stirred at room temperature for 2 h. The final solution had the molar ratio composition of  $\text{Zn}^{2+}$ : Hmim: DMF:  $\text{NH}_3=1: 2: 41: 30$ . In the end, the final mixture was centrifuged (5000 rpm, 30 min) and the recovered solid was washed with methanol three times. The obtained solid (ZIF-8) was dried at  $110^\circ\text{C}$  for 12 h to remove any remaining methanol.

The Fe species were impregnated on the ZIF-8 nanocatalyst through a rotary evaporator. The process involved four steps at several temperatures

Table 1. General information of PHP

Structure	Formula	Molar Mass (g.gmol <sup>-1</sup> )	$\lambda_{\max}$ (nm)	pKa
	C <sub>11</sub> H <sub>11</sub> N <sub>5</sub>	213.24	430	5.15

(65-75 °C) and pressures (200-300 mmHg) for 120 min. The corresponding intervals were 5 °C, 50 mmHg, and 30 min. Subsequently, the drying and calcination were at 105 °C and 530 °C overnight, respectively. The reduction process was applied using NaBH<sub>4</sub> and NaOH solution (NaBH<sub>4</sub>/NaOH=1.5 w/w), which was added to the impregnated powder and mixed for 10 min. Finally, the mixture was centrifuged and dried at 110°C overnight in order to obtain Fe-ZIF-8 nanocatalyst.

The detail of characterization methods was provided in the supplementary information.

#### HEF process

To measure the PHP removal, the experiments were carried out in a 100 ml bubble reactor. The graphite electrodes (3×2×0.5 cm) were attached to a DC power supply and immersed partially in the synthetic PHP wastewater solution, including 50 ml of PHP (10ppm), 0.05 M of Na<sub>2</sub>SO<sub>4</sub> as an electrolyte, and the specified amount of the Fe-ZIF-8 nanocatalyst. The pH of the solution was adjusted using a 0.01 M solution of H<sub>2</sub>SO<sub>4</sub> or NaOH. Before connecting the electrical current between electrodes, the solution was saturated with air for 5 min. During the experiments, aliquot samples were taken every 15 min. After centrifuging the samples, the concentration of PHP was calculated according to Eq.(1) using a UV-Vis spectrophotometer (i3, Jinan Hanon Instrument Co. Ltd, China) at 431 nm wavelength.

$$\%PHP\ removal = \frac{C_0 - C_t}{C_0} \times 100 \quad (1)$$

where C<sub>0</sub> is the initial PHP concentration and C<sub>t</sub> is the concentration of PHP in the taken samples.

## RESULTS AND DISCUSSIONS

### Nanocatalysts characterization

#### XRD

The index peaks of ZIF-8 (Fig. 1) appear at

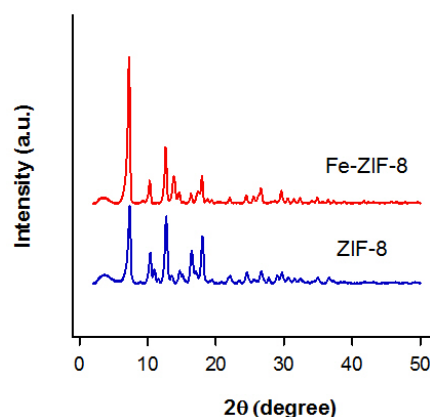


Fig. 1. XRD pattern of the ZIF-8 and Fe-ZIF-8 nanocatalysts.

29.7, 10.32, 12.65, 16.50, and 18.18°, which are related to the (011), (022), (112), (022), (013), (222), (114), (233), (134), (044), (244) and (235) planes, respectively [19]. The XRD pattern of the synthesized sample is in agreement with the reference XRD pattern of ZIF-8 [26] that confirms the synthesis of ZIF-8. The compatible pattern of the Fe-ZIF-8 and ZIF-8 samples represents a lack of significant framework destruction through the impregnation process. The XRD peaks are intensified after modification owing to the removal of some impurities from the parent structure, which is in line with the literature [27]. There are no peaks related to Fe<sub>3</sub>O<sub>4</sub> (JCPDS 19-629) in the Fe-ZIF-8 pattern, indicating a very strong interaction in the metal solution and uniform dispersion of Fe species on the ZIF-8 structure.

#### BET

The specific surface of the nanocatalysts depends on various parameters, including the raw materials, molar composition, and synthesis conditions. Fig. 2a shows the nitrogen adsorption-desorption isotherm for the synthesized ZIF-8 and Fe-ZIF-8 nanocatalysts. The isotherm of the

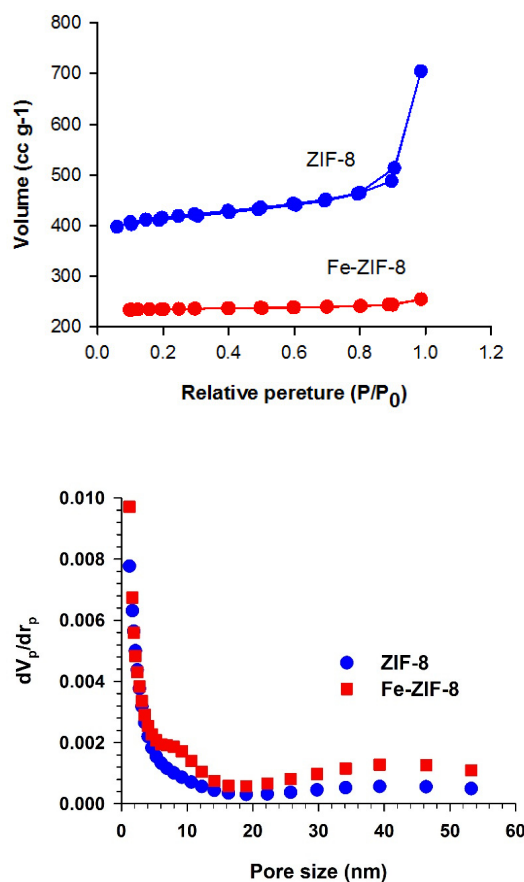


Fig. 2. a)  $N_2$  adsorption-desorption isotherm and b) pore size distribution of the ZIF-8 and Fe-ZIF-8 nanocatalysts.

Table 2 Textural data of the nanocatalysts

Sample	$S_{BET}$ ( $m^2g^{-1}$ )	$V_{Total}$ ( $cm^3g^{-1}$ )	Mean pore diameter (nm)
ZIF-8	1335.00	0.64	1.73
Fe-ZIF-8	714.30	0.35	2.08

nanocatalysts is Langmuir type I. Table 2 shows the calculated data for the samples. The synthesized ZIF-8 has a high surface area ( $1335 m^2g^{-1}$ ) and a pore volume ( $0.64 cm^3g^{-1}$ ), which are decreased for the Fe-ZIF-8 nanocatalyst. Furthermore, the impregnation increases the mean pore size distribution by the creation of some mesopores (Fig. 2b). This phenomenon could be explained by the slight framework destruction through the reduction step of the impregnation process [28]. Morabito et al. [29] found that ZIF-8 included a flexible framework due to the dissociation and association of linkers in an aqueous solution.

#### FT-IR

The FTIR spectrum of the ZIF-8 and Fe-ZIF-8 samples is shown in Fig. 3. The original core groups were identified correctly in the ZIF-8 sample [30], indicating that the ZIF-8 sample was properly synthesized and also support the XRD results. The peaks at  $2929$ ,  $3130$ , and  $3500 cm^{-1}$  are assigned to the aliphatic and aromatic C-H stretching vibration of the imidazole, and the stretching vibration of -OH, respectively [31]. The peaks at  $1200$ ,  $1600$ ,  $1674 cm^{-1}$  are attributed to the stretching vibration of C-N, C=N, and C=C. It is worth noting that the modification of ZIF-8 particles leads to the

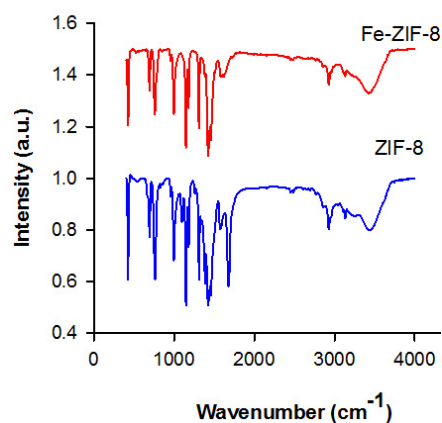


Fig. 3. FTIR spectrum of the ZIF-8 and Fe-ZIF-8 nanocatalysts.

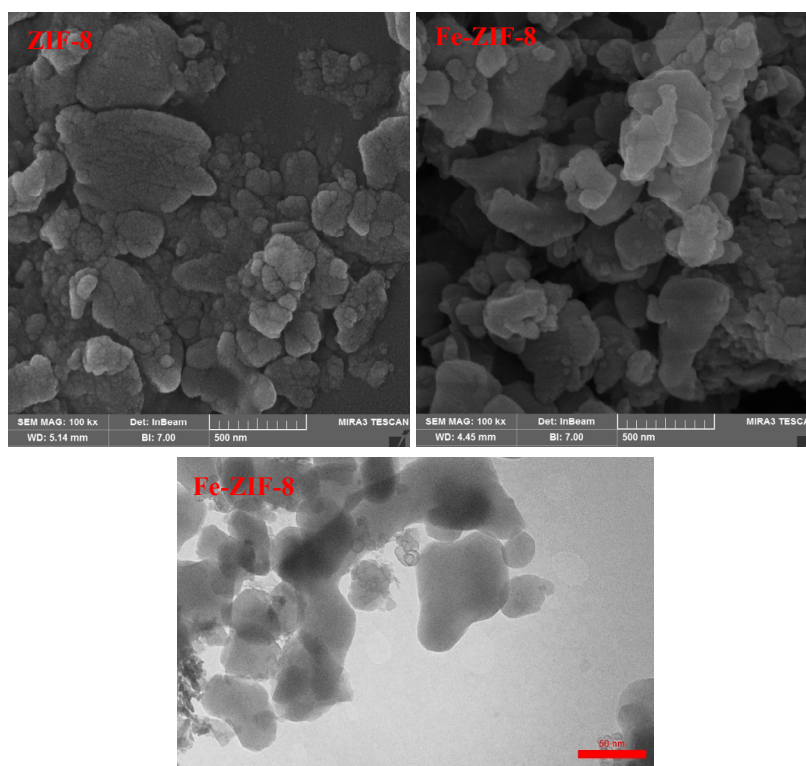


Fig. 4. FE-SEM and TEM images of the nanocatalysts.

decrease in intensity of absorbing bands and elimination of the peak related to C=C. The peaks at 1350–1500  $\text{cm}^{-1}$  have resulted from the entire ring stretching. The peaks around 900–1330  $\text{cm}^{-1}$  and 1440  $\text{cm}^{-1}$  are related to the imidazole ring. The peak at 462  $\text{cm}^{-1}$  is assigned to Zn–N stretch mode [32]. The absorbing band at 628  $\text{cm}^{-1}$  is attributed to Fe–N bands, confirming Fe incorporation in the synthesized adsorbent [33].

#### SEM and TEM

Fig. 4 shows that the ZIF-8 surface morphology consists of spherical particles with aggregation. It is clear that the surface morphology does not change significantly during the impregnation process. Furthermore, TEM images support the FE-SEM results and represent the formation of nanostructure with nano-scale particle size. The results are inconsistent with the literature [32].

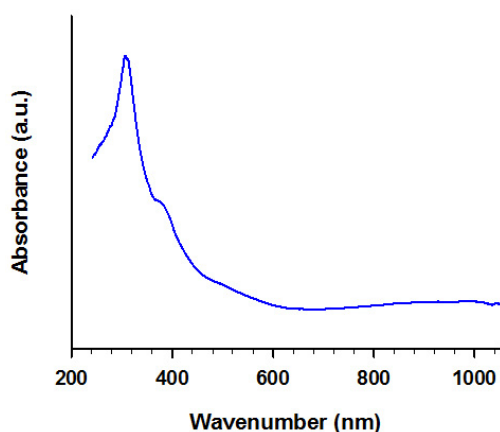


Fig. 5. DRS pattern of the Fe-ZIF-8 nanocatalyst.

### DRS

The different nature of iron species is detectable from the UV-vis spectrum. The peak in the 200-300 nm characterizes isolated Fe with tetrahedral or higher coordination.  $Fe_xO_y$  iron oxide oligomers are detected in the range of 300-400 nm. The presence of any peaks higher than 400 nm is usually attributed to large  $Fe_2O_3$  particles. According to the UV-vis spectrum for the Fe-ZIF-8 nanocatalyst (Fig. 5), a sharp peak is detected in the range of 300-400 nm. Therefore, iron species in the Fe-ZIF-8 nanocatalyst are in the form of small and uniformly distributed iron oxide clusters ( $Fe_3O_4$  or  $\gamma-Fe_2O_3$ ), which is consistent with the XRD results.

### Catalytic performance

Fig. 6 shows the performance of the Fe-ZIF-8 in the HEF system in comparison with anodic oxidation (AO), PHP adsorption on the Fe-ZIF-8 nanocatalyst, and the blank HEF process with no amount of the nanocatalyst at reaction conditions of pH=7, 25°C, and 100mA. Adsorption of PHP molecules on the outer and inner surface of the Fe-ZIF-8 nanoparticles can be through hydrogen bonding, Van der Waals, electrostatic, and  $\pi-\pi$  interactions. The low PHP removal by the adsorption process confirms the significant role of the developed nanocatalyst. The results show that the parent ZIF-8 nanocatalyst is not active in the HEF process. Fe loading on the ZIF-8 structure increases the performance of the nanocatalyst in the HEF process. The HEF process using the Fe-ZIF-8 nanocatalyst results in 99% PHP removal. This phenomenon can be explained by anodic oxidation at the surface of anode (M) (Eq.2) [9]

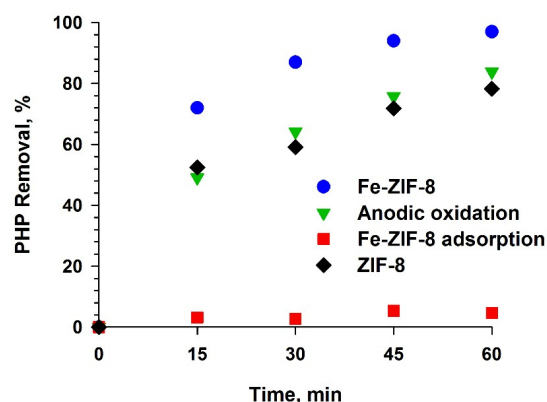
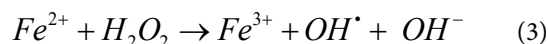
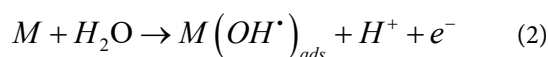


Fig. 6. Comparison of the ZIF-8 and Fe-ZIF-8 nanocatalysts. Reaction conditions: 0.1 A, pH= 7, [catalyst]=0.2 gL<sup>-1</sup>, and [PHP]= 10 ppm.

and Fenton reaction by electro-generated Fenton's reagent (Eq. 3) [34].



PHP removal mainly results from the reaction of the PHP molecules with  $OH^*$  radicals, which are produced through the Fenton reaction. *In-situ* electro-generated  $H_2O_2$  on the surface of graphite cathode (Eq. 4) diffuses into the bulk of the reaction medium as well as the structure of the Fe-ZIF-8 nanocatalyst.



The active iron species of the Fe-ZIF-8 nanocatalyst, in the form of nano-sized iron oxide clusters ( $Fe_3O_4$  or  $\gamma-Fe_2O_3$ ) according to the DRS results [35], react with  $H_2O_2$  and produce highly oxidative  $OH^*$  ( $E_v:2.80$  eV) radicals. The formed iron species include cubic inverse spinel structures such as magnetite that contains Fe cations with tetrahedral and octahedral sites. It is reported that octahedral sites include  $Fe^{2+}$  and tetrahedral sites include both  $Fe^{2+}$  and  $Fe^{3+}$  [36], resulting in oxidation and reduction ability of Fe species [37, 38]. Therefore, it is expected that the Fe-ZIF-8 nanocatalyst is regenerated electrically in the reaction solution through the HEF system (Eq.5) [39].



However,  $Fe^{2+}$  consumption (Eq. 3) occurs at a

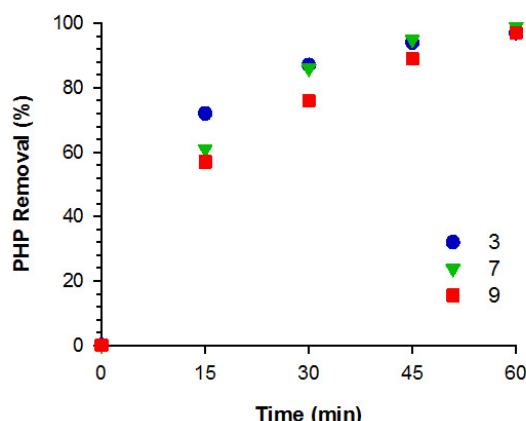
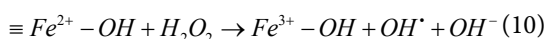
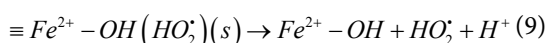
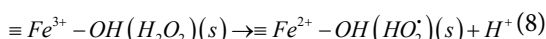
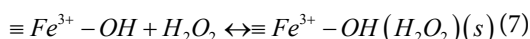
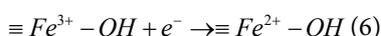


Fig. 7. Effect of pH on the PHP removal efficiency. Reaction conditions: 0.1 A, [catalyst]=0.2 gL<sup>-1</sup>, and [PHP]=10 ppm

higher rate than its regeneration (Eq. 5) which is in line with the high PHP removal at the beginning.

It is stated in the literature that the kinetics of the HEF process and activation of H<sub>2</sub>O<sub>2</sub> onto heterogeneous reactive iron oxide sites are very complex. Wang et al. [37] proposed that the HEF kinetics simply fits the well-known Haber-Weiss mechanism as follows:



#### Effect of pH

The pH parameter controls the amount of radical hydroxyl production and the concentration of ionic ferrous in the solution. Hence, pH is one of the most important parameters in the HEF process. When the pH increases, the precipitation of Fe<sup>3+</sup> ions increases, preventing the formation of Fe<sup>2+</sup> ions so the reaction efficiency drops. H<sub>2</sub>O<sub>2</sub> is also unstable at pH= 5 and rapidly converts to hydrogen and oxygen so the high alkalinity reduces H<sub>2</sub>O<sub>2</sub> stability and iron ion deposition. At pH < pH<sub>pzc</sub>, the proton on the surface leads to a positive charge. But at pH > pH<sub>pzc</sub>, the proton deficiencies result in a negative charge. In contrast, the existence of protons on the surface of the acidic materials neutralizes the compound at pH < pH<sub>pKa</sub>,

but it is negatively charged by the loss of proton at pH > pH<sub>pKa</sub>. The basic materials are neutralized by taking proton at a pH < pH<sub>pKa</sub> and positively charged with a loss of proton at pH > pH<sub>pKa</sub>.

By comparing the catalytic performance of the Fe-ZIF-8 nanocatalyst at different pH (Fig. 7), it is clear that pH=3 results in the highest PHP removal. At pH=7, a sharp reduction of OH<sup>•</sup> oxidation ability and conversion of H<sub>2</sub>O<sub>2</sub> to water hinder the HEF efficiency. However, the enhanced adsorption of the PHP molecules onto the Fe-ZIF-8 particles as a result of electrostatic forces between the positively charged Fe-ZIF-8 particles (pH<sub>pzc</sub>=8) and the negatively charged PHP molecules (pKa=5.15), improves the efficiency of the HEF system. Since operation at neutral pH is conducted with the addition of no acid and alkali compounds. Therefore, pH=7 is selected as the optimum pH for the other experiments, which can be the best pH both economically and environmentally. Furthermore, this result also proposes that the main drawback of Fenton and Fenton-like reactions (strict acidic pH control) can be addressed through the utilization of the Fe-ZIF-8 nanocatalyst at neutral pH in the HEF system.

#### Effect of nanocatalyst concentration

The nanocatalyst concentration is a very important parameter for controlling the removal efficiency in the Fenton and Fenton-like reactions. Increasing the concentration of the nanocatalyst increases the rate of radical hydroxyl production as well as the removal efficiency removal of PHP. The excessive nanocatalyst concentration raises the probability of the nanocatalyst present on the surface of the graphite cathode and reduces

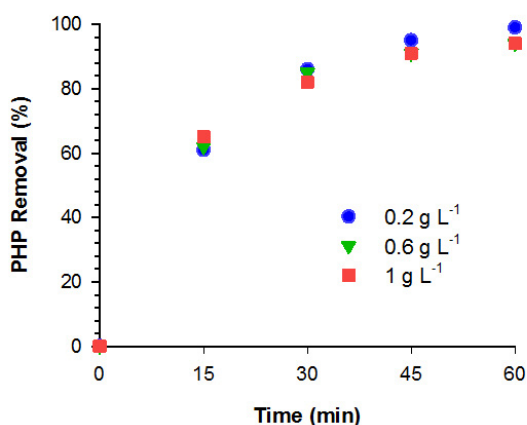


Fig. 8. Effect of the nanocatalyst concentration on the PHP removal efficiency. Reaction conditions: 0.1 A, pH=7, and [PHP] =10 ppm.

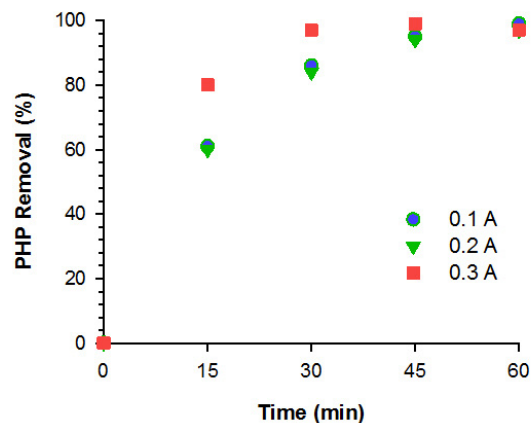


Fig. 9. Effect of the applied current on the PHP removal efficiency. Reaction conditions: pH = 7, [catalyst]=0.2 g L<sup>-1</sup>, and [PHP] =10 ppm.

the volume of the cathode pores as well as the production of H<sub>2</sub>O<sub>2</sub> [40, 41]. Furthermore, the high concentration of iron has a negative effect on the process performance due to the side reaction (Eq. 11).

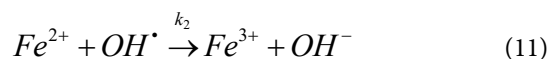
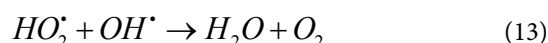
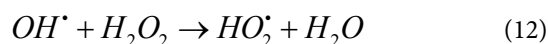


Fig. 8 shows that the PHP removal efficiency reduces from 99% to 94% in 60 min by increasing the Fe-ZIF-8 nanocatalyst from 0.2 to 0.6 gL<sup>-1</sup>. However, the increase of the nanocatalyst concentration from 0.6 to 1 gL<sup>-1</sup> does not change the efficiency (94%). Therefore, the nanocatalyst concentration of 0.2 gL<sup>-1</sup> is the optimum concentration.

#### Effect of applied current

We conducted the HEF experiments with three different applied current levels. Fig. 9 shows that the increase of the current from 0.1 to 0.2 A leads to a loss of efficiency owing to the production of additional H<sub>2</sub>O<sub>2</sub>, which reacts with radical hydroxyl and leads to its destruction. The high current promotes the side reactions: i) excessive H<sub>2</sub>O<sub>2</sub> generation, ii) transformation radical hydroxyl into the weaker oxidative (HO<sub>2</sub>•), iii) HO<sub>2</sub>• reaction with OH• (Eqs. 12-13) [42, 43]. Bagheri et al. [10] applied different current for the purification of formaldehyde (0.85 mA.Cm<sup>-2</sup> to 17 mA.cm<sup>-2</sup>) and found the current of 8.5mA.cm<sup>-2</sup> as the optimum. The process efficiency is improved by the excessive current (0.3A) owing to the increase of the reaction between the electrodes and the rate of iron ion production on the anode but destroy the cathode.

Therefore, the current of 0.1A is selected as the optimum value, resulting in the high and durable performance of the process.



#### Effect of PHP concentration

Fig. 10 shows that the high concentration of PHP leads to low removal efficiency. This result can be clarified by the constant amount of active hydroxyl radicals, hindering the degradation of pollutants within the excess amount of PHP. The high concentration of PHP would consume more OH• radicals, so the effect would be decreased with the high initial concentration of PHP. Saeid et al. [44] investigated the effect of PHP concentration in the range of 20-50 mgL<sup>-1</sup> in the UV/H<sub>2</sub>O<sub>2</sub> process. The results showed that the process efficiency decreased with the increase of PHP concentration. Furthermore, the non-specific oxidation of major intermediates with OH• radicals may result in the side reactions and the competitive consumption of OH• radicals [45].

#### Kinetic

Pseudo-First-Order kinetic model well describes the PHP degradation data. The kinetic is according to Eq. (14).

$$\ln\left(\frac{C}{C_0}\right) = -kt \quad (14)$$

where C and C<sub>0</sub> (mg L<sup>-1</sup>) are the residual and

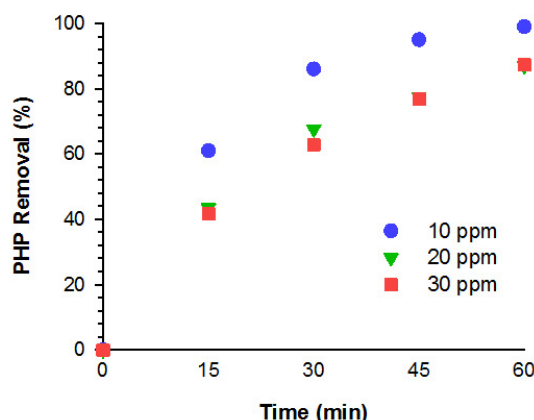


Fig. 10. Effect of the pollutant concentration on the PHP removal efficiency. Reaction conditions: pH = 7, 0.1 A, and [catalyst]=0.2 g L<sup>-1</sup>.

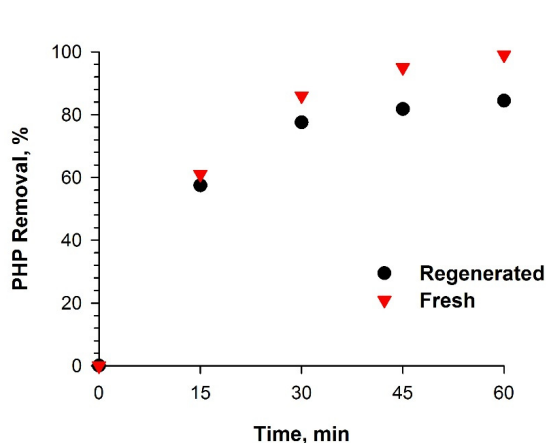


Fig. 12. Reusability of the nanocatalyst. Reaction conditions: pH = 7, 0.1 A, [PHP] =10 ppm, and [catalyst]=0.2 g L<sup>-1</sup>.

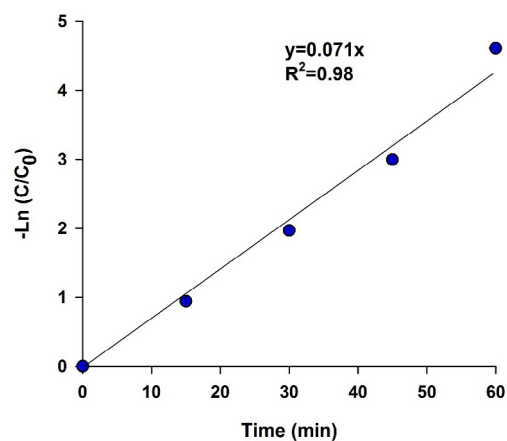


Fig. 11. Kinetic of PHP degradation at optimum operating conditions: pH = 7, 0.1 A, [PHP] =10 ppm, and [catalyst]=0.2 g L<sup>-1</sup>.

Table 3 Comparison of the PHP removal in different processes

Catalyst	Process	pH	PHP concentration (ppm)	Catalyst concentration (g L <sup>-1</sup> )	Removal (%)	Ref.
Clinoptilolite	Electro-Fenton	5	10	2	90.1	[22]
Ag/SiO <sub>2</sub> -TiO <sub>2</sub>	Photocatalytic	-	10	40	97.1	[23]
Sm-ZnO	Sonocatalytic	-	10	1	90	[25]
No catalyst	Electro-Fenton	3	20	-	98.4	[46]
No catalyst	Electro-Fenton	3	30	-	98.2	[47]
SnO <sub>2</sub> -BiVO <sub>4</sub>	Photocatalytic	7.2	10	0.5	90	[48]
CuO-SnO <sub>2</sub>	Photocatalytic	7	5.5	0.8	89.7	[49]
Fe-ZIF-8	Electro-Fenton	7	10	0.2	99	This work

initial PHP concentrations, respectively.  $k$  (min<sup>-1</sup>) is the constant of Pseudo-First-Order kinetic and  $t$  (min) is the reaction time. Fig. 11 shows the kinetic of PHP degradation at optimum operating conditions. The results confirm that the proposed kinetic model is in line with the experimental data.

#### Reusability

Fig. 12 represents the application of the Fe-

ZIF-8 nanocatalyst for the PHP removal in the sequence runs. The spent nanocatalyst was washed with methanol to remove the adsorbed organic molecules and dried at 105°C overnight. The regenerated nanocatalyst was evaluated at the optimum operating conditions: pH=7 applied current of 0.1A, the nanocatalyst concentration of 0.2 gL<sup>-1</sup>, and PHP concentration of 10 ppm. The results prove the high reusability of the Fe-

ZIF-8 nanocatalyst in the sequence runs. The stability of the nanocatalyst depends on diverse factors, including the exit of pollutant molecules and oxidized intermediates from pores that are accelerated by the high surface area and total pore volume.

Table 3 compares the PHP removal over the developed Fe-ZIF-8 nanocatalyst with the literature. It is clear that the high performance and applicable operating conditions, including neutral pH and low catalyst concentration, result from the appropriate physicochemical properties of the Fe-ZIF-8 nanocatalyst.

## CONCLUSION

The ZIF-8 nanocatalyst was synthesized using the thermal solvent method and doped with an iron promoter through the multi-step impregnation technique. The characterization showed the high surface area and uniform dispersion of Fe species on the ZIF-8 nanocatalyst. The synthesized Fe-ZIF-8 nanocatalyst was applied for the PHP removal in the HEF process at different operating conditions. The results showed that the highest PHP removal efficiency (99%) was obtained at a pH of 7, nanocatalyst concentration of 0.2 gL<sup>-1</sup>, and applied current of 0.1 A. Furthermore, the nanocatalyst showed high reusability due to its proper properties. The results confirmed the high potential of the ZIF-8 nanocatalyst for wastewater treatment applications.

## ACKNOWLEDGMENTS

The authors also wish to acknowledge the Sahand University of Technology for its support of this study.

## CONFLICTS OF INTEREST

The authors declare there are no conflicts of interest.

## REFERENCES

- Adel Niaei H, Rostamizadeh M. Adsorption of metformin from an aqueous solution by Fe-ZSM-5 nano-adsorbent: Isotherm, kinetic and thermodynamic studies. *The Journal of Chemical Thermodynamics*. 2020;142:106003.
- Lin C-C, Lee C-Y. Adsorption of ciprofloxacin in water using Fe<sub>3</sub>O<sub>4</sub> nanoparticles formed at low temperature and high reactant concentrations in a rotating packed bed with co-precipitation. *Materials Chemistry and Physics*. 2020;240:122049.
- Abbasi AR, Hatami S. Comparison of Structure of Nano Zinc Metal-Organic Frameworks Upon Uptake and Release of Phenazopyridine Hydrochloride. *Journal of Inorganic and Organometallic Polymers and Materials*. 2017;27(6):1941-9.
- Ronald KE, Demissie A. Phenazopyridine-Induced Toxicity in an Elderly Patient Receiving a Prolonged Regimen of Therapeutic Doses. *Journal of Pharmacy Technology*. 2013;29(3):130-4.
- Tian J, Sharshar MM, Yang M, Mu T, Xing J. Degradation of Rhodamine B at neutral pH using modified sponge iron as a heterogeneous electro-Fenton catalyst. *Environmental Progress & Sustainable Energy*. 2017;37(3):989-95.
- Saini R, Kumar Mondal M, Kumar P. Fenton oxidation of pesticide methyl parathion in aqueous solution: kinetic study of the degradation. *Environmental Progress & Sustainable Energy*. 2016;36(2):420-7.
- Rostamizadeh M, Jafarizad A, Gharibian S. High efficient decolorization of Reactive Red 120 azo dye over reusable Fe-ZSM-5 nanocatalyst in electro-Fenton reaction. *Separation and Purification Technology*. 2018;192:340-7.
- Dolatabadi M, Ahmadzadeh S, Ghaneian MT. Mineralization of mefenamic acid from hospital wastewater using electro-Fenton degradation: Optimization and identification of removal mechanism issues. *Environmental Progress & Sustainable Energy*. 2019;39(3).
- Lin H, Oturan N, Wu J, Sharma VK, Zhang H, Oturan MA. Removal of artificial sweetener aspartame from aqueous media by electrochemical advanced oxidation processes. *Chemosphere*. 2017;167:220-7.
- Bagheri, A., Moussavi, G., and Khavanin, A. 2012. Investigating the Electro-Fenton (EF) process performance in treating highly formaldehyde-polluted industrial wastewater. *IJHE*, 5, 143-156.
- Vosoughi M, Fatehifar E, Derafshi S, Rostamizadeh M. High efficient treatment of the petrochemical phenolic effluent using spent catalyst: Experimental and optimization. *Journal of Environmental Chemical Engineering*. 2017;5(2):2024-31.
- Li K, Olson DH, Seidel J, Emge TJ, Gong H, Zeng H, et al. Zeolitic Imidazolate Frameworks for Kinetic Separation of Propane and Propene. *Journal of the American Chemical Society*. 2009;131(30):10368-9.
- Isaeva VI, Kustov LM. Metal-Organic Frameworks and Related Materials. *Zeolites and Zeolite-Like Materials*: Elsevier; 2016. p. 33-109.
- Alvaro M, Carbonell E, Ferrer B, Llabrés i Xamena FX, Garcia H. Semiconductor Behavior of a Metal-Organic Framework (MOF). *Chemistry - A European Journal*. 2007;13(18):5106-12.
- Andrew Lin K-Y, Hsieh Y-T. Copper-based metal organic framework (MOF), HKUST-1, as an efficient adsorbent to remove p-nitrophenol from water. *Journal of the Taiwan Institute of Chemical Engineers*. 2015;50:223-8.
- Haque E, Lee JE, Jang IT, Hwang YK, Chang J-S, Jegal J, et al. Adsorptive removal of methyl orange from aqueous solution with metal-organic frameworks, porous chromium-benzenedicarboxylates. *Journal of Hazardous Materials*. 2010;181(1-3):535-42.
- Lee Y-R, Jang M-S, Cho H-Y, Kwon H-J, Kim S, Ahn W-S. ZIF-8: A comparison of synthesis methods. *Chemical Engineering Journal*. 2015;271:276-80.
- Pan Y, Liu Y, Zeng G, Zhao L, Lai Z. Rapid synthesis of zeolitic imidazolate framework-8 (ZIF-8) nanocrystals in an aqueous system. *Chemical Communications*. 2011;47(7):2071.

19. Thi Thanh M, Vinh Thien T, Thi Thanh Chau V, Dinh Du P, Phi Hung N, Quang Khieu D. Synthesis of Iron Doped Zeolite Imidazolate Framework-8 and Its Remazol Deep Black RGB Dye Adsorption Ability. *Journal of Chemistry*. 2017;2017:1-18.
20. Pan Y, Li Z, Zhang Z, Tong X-S, Li H, Jia C-Z, et al. Adsorptive removal of phenol from aqueous solution with zeolitic imidazolate framework-67. *Journal of Environmental Management*. 2016;169:167-73.
21. Wu Y-n, Zhou M, Zhang B, Wu B, Li J, Qiao J, et al. Amino acid assisted templating synthesis of hierarchical zeolitic imidazolate framework-8 for efficient arsenate removal. *Nanoscale*. 2014;6(2):1105-12.
22. Khataee A, Rad TS, Vahid B, Khorram S. Preparation of zeolite nanorods by corona discharge plasma for degradation of phenazopyridine by heterogeneous sono-Fenton-like process. *Ultrasonics Sonochemistry*. 2016;33:37-46.
23. Eskandarloo H, Badieli A, Behnajady MA, Afshar M. Enhanced photocatalytic removal of phenazopyridine by using silver-impregnated SiO<sub>2</sub>-TiO<sub>2</sub> nanoparticles: optimization of synthesis variables. *Research on Chemical Intermediates*. 2015;41(12):9929-49.
24. Abbasi AR, Karimi M, Masoomi MY. Effect of construction method and surface area for nano metal-organic framework HKUST-1 upon adsorption and removal of phenazopyridine hydrochloride. *Colloids and Surfaces A: Physicochemical and Engineering Aspects*. 2017;520:193-200.
25. Eskandarloo H, Badieli A, Behnajady MA, Ziarani GM. Ultrasonic-assisted degradation of phenazopyridine with a combination of Sm-doped ZnO nanoparticles and inorganic oxidants. *Ultrasonics Sonochemistry*. 2016;28:169-77.
26. Schejn A, Balan L, Falk V, Aranda L, Medjahdi G, Schneider R. Controlling ZIF-8 nano- and microcrystal formation and reactivity through zinc salt variations. *CrystEngComm*. 2014;16(21):4493-500.
27. Md Nordin NAH, Racha SM, Matsuura T, Misdan N, Abdullah Sani NA, Ismail AF, et al. Facile modification of ZIF-8 mixed matrix membrane for CO<sub>2</sub>/CH<sub>4</sub> separation: synthesis and preparation. *RSC Advances*. 2015;5(54):43110-20.
28. Liao Y-T, Chen JE, Isida Y, Yonezawa T, Chang W-C, Alshehri SM, et al. Cover Picture: De Novo Synthesis of Gold-Nanoparticle-Embedded, Nitrogen-Doped Nanoporous Carbon Nanoparticles (Au@NC) with Enhanced Reduction Ability (ChemCatChem 3/2016). *ChemCatChem*. 2016;8(3):473-.
29. Morabito JV, Chou L-Y, Li Z, Manna CM, Petroff CA, Kyada RJ, et al. Molecular Encapsulation beyond the Aperture Size Limit through Dissociative Linker Exchange in Metal-Organic Framework Crystals. *Journal of the American Chemical Society*. 2014;136(36):12540-3.
30. Tran UPN, Le KKA, Phan NTS. Expanding Applications of Metal-Organic Frameworks: Zeolite Imidazolate Framework ZIF-8 as an Efficient Heterogeneous Catalyst for the Knoevenagel Reaction. *ACS Catalysis*. 2011;1(2):120-7.
31. Hassani A, Soltani RDC, Karaca S, Khataee A. Preparation of montmorillonite-alginate nanobiocomposite for adsorption of a textile dye in aqueous phase: Isotherm, kinetic and experimental design approaches. *Journal of Industrial and Engineering Chemistry*. 2015;21:1197-207.
32. Sajjadi S, Khataee A, Darvishi Cheshmeh Soltani R, Bagheri N, Karimi A, Ebadi Fard Azar A. Implementation of magnetic Fe<sub>3</sub>O<sub>4</sub>@ZIF-8 nanocomposite to activate sodium percarbonate for highly effective degradation of organic compound in aqueous solution. *Journal of Industrial and Engineering Chemistry*. 2018;68:406-15.
33. Zhang X, Liu Y, Jiao Y, Gao Q, Wang P, Yang Y. Enhanced selectively removal uranyl ions from aqueous solution by Fe@ZIF-8. *Microporous and Mesoporous Materials*. 2019;277:52-9.
34. Özcan A, Atlı Ö, Demirci Y. Evaluation of mineralization kinetics and pathway of norfloxacin removal from water by electro-Fenton treatment. *Chemical Engineering Journal*. 2016;304:518-26.
35. Li C, Ma C, Wang F, Xi Z, Wang Z, Deng Y, et al. Preparation and Biomedical Applications of Core-Shell Silica/Magnetic Nanoparticle Composites. *Journal of Nanoscience and Nanotechnology*. 2012;12(4):2964-72.
36. Rakibuddin M, Kim H. Sol-gel derived Fe<sub>3</sub>O<sub>4</sub> quantum dot decorated silica composites for effective removal of arsenic (III) from water. *Materials Chemistry and Physics*. 2020;240:122245.
37. Wang Y, Zhao H, Chai S, Wang Y, Zhao G, Li D. Electrosorption enhanced electro-Fenton process for efficient mineralization of imidacloprid based on mixed-valence iron oxide composite cathode at neutral pH. *Chemical Engineering Journal*. 2013;223:524-35.
38. Jafarizad A, Rostamizadeh M, Zarei M, Gharibian S. Mitoxantrone removal by electrochemical method: A comparison of homogenous and heterogeneous catalytic reactions. *Environmental Health Engineering and Management*. 2017;4(4):185-93.
39. Nidheesh PV, Gandhimathi R, Velmathi S, Sanjini NS. Magnetite as a heterogeneous electro Fenton catalyst for the removal of Rhodamine B from aqueous solution. *RSC Advances*. 2014;4(11):5698.
40. Nidheesh PV, Gandhimathi R. Comparative Removal of Rhodamine B from Aqueous Solution by Electro-Fenton and Electro-Fenton-Like Processes. *CLEAN - Soil, Air, Water*. 2013;42(6):779-84.
- [41] Rostamizadeh, M., Jalali, H., Naeimzadeh, F., and Gharibian, S. 2019. Efficient Removal of Diclofenac from Pharmaceutical Wastewater Using Impregnated Zeolite Catalyst in Heterogeneous Fenton Process. *Phys. Chem. Res.*, 7, 37-52.
42. Hou B, Han H, Jia S, Zhuang H, Xu P, Wang D. Heterogeneous electro-Fenton oxidation of catechol catalyzed by nano-Fe<sub>3</sub>O<sub>4</sub>: kinetics with the Fermi's equation. *Journal of the Taiwan Institute of Chemical Engineers*. 2015;56:138-47.
43. Gharibian S, Hazrati H, Rostamizadeh M. Continuous electrooxidation of Methylene Blue in filter press electrochemical flowcell: CFD simulation and RTD validation. *Chemical Engineering and Processing - Process Intensification*. 2020;150:107880.
44. Saeid S, Behnajady M. Photooxidative Removal of Phenazopyridine by UV/H<sub>2</sub>O<sub>2</sub> Process in a Batch Re-circulated Annular Photoreactor: Influence of Operational Parameters. *Oriental Journal of Chemistry*. 2015;31(2):1211-4.
45. Murugananthan M, Yoshihara S, Rakuma T, Shirakashi T. Mineralization of bisphenol A (BPA) by anodic oxidation with boron-doped diamond (BDD) electrode. *Journal of Hazardous Materials*. 2008;154(1-3):213-20.
46. Gholizadeh AM, Zarei M, Ebratkhanan M, Hasanizadeh A, Vafaei F. Removal of Phenazopyridine from wastewater

- by merging biological and electrochemical methods via *Azolla filiculoides* and electro-Fenton process. *Journal of Environmental Management*. 2020;254:109802.
47. Gholizadeh AM, Zarei M, Ebratkhahan M, Hasanzadeh A. Phenazopyridine degradation by electro-Fenton process with magnetite nanoparticles-activated carbon cathode, artificial neural networks modeling. *Journal of Environmental Chemical Engineering*. 2021;9(1):104999.
48. Yousefi A, Nezamzadeh-Ejhieh A, Mirmohammadi M. SnO<sub>2</sub>-BiVO<sub>4</sub> mixed catalyst: Characterization and kinetics study of the photodegradation of phenazopyridine. *Environmental Technology & Innovation*. 2021;22:101433.
49. Yousefi A, Nezamzadeh-Ejhieh A, Mirmohammadi M. The coupled CuO-SnO<sub>2</sub> catalyst: Characterization and the photodegradation kinetics towards phenazopyridine. *Environmental Technology & Innovation*. 2021;22:101496.